Atomization and Sprays, vol. 1, pp. 113–136, 1991

EFFECT OF SHOCK WAVES ON LIQUID ATOMIZATION OF A TWO-DIMENSIONAL AIRBLAST ATOMIZER

K. D. Kihm
Mechanical Engineering Department,
Texas A&M University, College Station, Texas 77843

N. Chigier
Mechanical Engineering Department,
Carnegie Mellon University, Pittsburgh, Pennsylvania 15213

Two major questions have been raised by the designers of airblast fuel atomizers: (1) When the atomizing air is choked and underexpanded through a convergent nozzle, do shock waves exist in the presence of liquid? (2) If so, will these shock waves enhance the efficiency and performance of sonic air-blast atomizers? A two-dimensional twin air-blast research atomizer was designed and carefully machined to study these questions and demonstrate the influence of shock waves on atomization processes. Using a shadowgraph technique, shock wave patterns have been visualized with and without liquid injection. The shock wave patterns have also been studied theoretically based on the isentropic flow assumption and the Prandtl-Meyer expansion fan. Droplet size distributions have been measured for both subsonic and sonic conditions by the Malvern Fraunhofer diffraction particle sizing technique for water sprays using air as the atomizing fluid. Measurements of Sauter mean diameter (SMD) were made as a function of the air-to-liquid velocity and mass ratios for several different orifice dimensions of air and liquid flows. The Mach number in the shock cells was varied up to 1.5 as the upstream stagnation pressure was progressively increased. It was found that the velocity of the air relative to the liquid has the most important influence on mean drop size variation. The SMD shows a rapid decrease with increase in the relative velocity as the air jets approach the sonic condition. Near choking and after the flow is choked, SMD decreases very slowly, whereas the density-weighted relative velocity, $\bar{\rho}V_{rel}$, progressively increases with the stagnation pressure. For the fine atomizer that we employed, a critical Weber number We_{crit} was already attained near the choking condition, and a further reduction in SMD was not apparent up to the local Mach number of 1.5. In order to investigate the effect of shock waves on airblast atomization more extensively, supersonic air jets of higher Mach number should be applied so that the Weber number can exceed the critical value after the flow is choked.

INTRODUCTION

In airblast atomizers, liquid fuel at low pressure is injected in the form of a thin film into a high-velocity airstream [1]. Aerodynamically disruptive waves with large amounts of kinetic energy and the momentum flux of high-velocity airstreams are the

The authors gratefully acknowledge the assistance of Peter Zion and Phillip Corbeels in conducting the experimental investigations. The authors extend special thanks to Harold Simmons at Parker Hannifin for his invaluable suggestions and encouragement. The research was conducted with financial assistance from Parker Hannifin Corporation, Cleveland, Ohio.

NOMENCLATURE

A	cross-sectional area of air nozzles, mm^2
D	drop diameter, μm
D_0	Rosin-Rammler distribution model parameter, μm
M	Mach number
$\dot{m}_{air}$	air mass flow rate, g/s
$\dot{m}_{liquid}$	liquid mass flow rate, g/s
n	number distribution function
P	air pressure, kPa
P_0	stagnation pressure, kPa
P_{0c}	critical stagnation pressure for choking, kPa
Q	volume fraction of drops with diameters less than D
q	Rosin-Rammler distribution model parameter
R	gas constant, 287.07 J/kg K for air
T	air temperature, K
t_{air}	air slit thickness, mm
t_{liquid}	liquid slit thickness, mm
U	mean velocity of air, m/s
V_{rel}	relative velocity of air with respect to liquid flows, m/s
We	Weber number ($= \rho U^2 D/\sigma$)
x	coordinate parallel to the gas flow direction
y	coordinate parallel to the liquid slit
z	coordinate perpendicular to the liquid slit
γ	specific heat ratio ($= 1.4$ for air)
ϵ	amount of light energy detected by the center diode in the detector unit of the Malvern
ϵ_0	amount of light energy detected in the absence of spray
ρ	air density
$\bar{\rho}$	density ratio of the air at the nozzle exit to the ambient air
σ	surface tension coefficient ($= 0.0735$ N/m for water at STP)
μ	absolute viscosity ($= 0.001$ kg/ms s for water)

Subscripts

1, 2, 3	regions separated by Prandtl-Meyer expansion fans and oblique shock waves in the supersonic air jets from a convergent air nozzle
i	ith size bin in diameter
g	gas state

primary forces in breaking up the liquid film into droplets. The advantages of airblast atomizers over the simple pressure atomizers, in which disruptive forces originate from the pressure force of the liquid, are well known, especially in their application to gas turbine combustors: (1) lower pressurization of liquid fuel, (2) finer spray, (3) more uniform combustion, and (4) lower soot formation. As noncombusting examples, modern painting, coating, and sintering industries use the airblast atomization technique more commonly because of these advantages.

In airblast atomizers, the air supply pressures are often sufficiently high to result in sonic conditions at the (convergent) nozzle exit (R. V. Jones, private communication, 1986). As exit Mach numbers exceed 0.4, compressibility effects can no longer be neglected. As sonic conditions are approached, the air flow at the nozzle exit becomes choked (Mach number = 1). Further increases in supply pressure result in underexpanded sonic jets with formation of expansion waves and oblique shocks. The goal of the present work is to study the physics of sonic air jets from both single and double convergent air nozzles and then to investigate the effects of these air jets on liquid atomization.

Despite its importance, airblast atomization in connection with underexpanded air jets has not been studied extensively. One of the most closely related studies is the investigation of aerodynamic shattering of liquid drops in the convective flow field established by a shock wave passing over them. Hanson et al. [2] investigated the

breakup of drops by airblast in a shock tube for several different liquids. They used photography to study details of the breakup process of liquid drops of several hundred micrometers. When a normal shock runs over a drop, shattering of the drop is caused by the relative velocity between drop and air, not by the shock wave itself. Ranger and Nicholls [3, 4] observed the breakup of droplets injected into a shock tube using a shadowgraphic visualization technique. Water drops having diameters of 750–4000 μm were allowed to interact with shock waves moving at Mach numbers ranging from 1.5 to 3.5 in air. They found that high-speed convective flow is responsible for the drop disintegration resulting in a fine mist and that the breakup time is proportional to the drop diameter and inversely proportional to the air flow velocity.

A similar technique was applied to observe the breakup and interaction of two droplet columns by Yoshida et al. [5]. For the condition in which shock waves pass over water droplets 1400 μm in diameter, they investigated the mutual interference effects of two neighboring droplets in a high-speed shock wave–induced air flow with a Mach number of 1.4. Compared to the case of a single drop, more complicated patterns of breakup and disintegration were observed with the two droplets.

Atomization processes of continuously flowing liquid films such as those in airblast atomizers involve interactions of millions of droplets having different sizes and shapes. Airblast atomization is a complicated process in which thin liquid films disintegrate into ligaments, which eventually break up into droplets as a result of shear forces exerted on the liquid surface. Thus, the aerodynamic shattering of single or multiple droplets of large diameter cannot be generalized or directly applied to describe the overall effect of shock waves on the performance of airblast atomizers.

For the case of subsonic air jets, the mean drop size distributions from airblast atomizers have been studied quantitatively by several investigators. Kim and Marshall [6] employed a molten-wax technique. Drop size was determined by counting and sizing the solidified wax particles using a microscope. Although their techniques for counting and sizing are now considered to be outdated, they succeeded in demonstrating that the mean drop size in a coarse spray (low air pressure) depends primarily on the air-to-liquid mass ratio, whereas the effects of relative velocity become dominant in sprays with high air pressures.

Using a light-scattering counting technique, Rizkalla and Lefebvre [7, 8] and Lorenzetto and Lefebvre [9] performed drop size measurements to investigate the effects of various parameters on airblast atomization quality. In addition to the conclusions drawn by Kim and Marshall [6], it was found that the mean drop size increases with increases in liquid viscosity and surface tension and decreases with increases in liquid density and air velocity. The effect of fuel orifice size on the atomization quality was found to be quite small.

Styles and Chigier [10] investigated the spatial distribution of drop mean diameters in a spray using a laser diffraction technique. They found that the mean drop size decreases in the initial region of the spray due to secondary atomization, whereas farther downstream, preferential vaporization of small droplets leads to increases in the mean diameter.

The influence of liquid film thickness on airblast atomization was examined by Rizk and Lefebvre [11], who measured the mean drop size while varying the liquid orifice gap size. Although they showed a weak dependence of the mean drop size on the film thickness, the orifice thickness was not varied independently in their examination.

Since the air gap size was also varied, their conclusion may reflect the combined effect of air and liquid film thickness variation.

In all of these studies of airblast atomizers, the air flow was subsonic with Mach numbers less than 0.4. In the present study, the air flow is high enough to generate nonadapted underexpanded jets [12], where the nozzle exit pressure is higher than the ambient pressure. This allows us to investigate the influence of the diamond-shaped succession of shock waves [13] on airblast atomization processes. For the investigation of fundamental mechanisms of atomization, a two-dimensional research airblast atomizer has been designed and carefully manufactured. Shock patterns from both single and double air jet streams have been studied using a shadowgraph visualization technique. For both subsonic and sonic air flows, atomization quality has been examined by individually varying the relevant parameters: air/liquid mass ratio, relative velocity between air and liquid, and atomizer dimensions. Drop size measurements were made of the Sauter mean diameter [14, 15] using the well-established Fraunhofer diffraction particle-sizing technique [16].

EXPERIMENTAL PROCEDURES

Two-Dimensional Airblast Atomizer

The two-dimensional airblast research atomizer is shown in Fig. 1. A liquid film emerges from the central slit with high aspect ratio (Table 1). High-pressure air impinges on either side of the liquid film at the nozzle exit. The liquid film is sandwiched between two high speed concurrent air jets. Although most practical atomizers have concentric nozzle configurations for both air and liquid, the two-dimensional research atomizer has special advantages, allowing more direct examination of air-liquid inter-

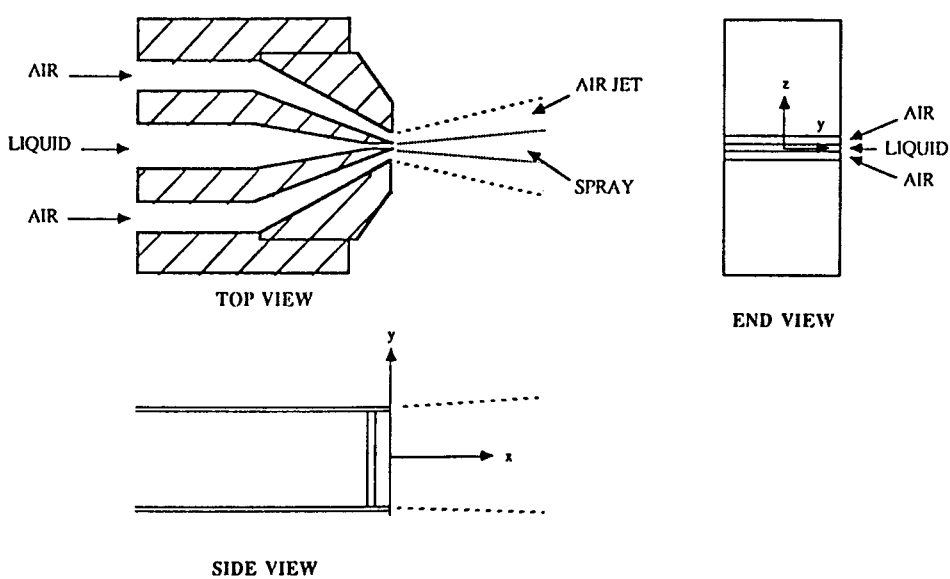

Fig. 1 Two-dimensional airblast research atomizer. Thickness of liquid and air films can be varied.

Table 1 Dimensions of Nozzles and Experimental Conditions

Dimensions of nozzles			
Air slit (mm)	Total flow area (m^2)	Liquid slit (mm)	Flow area (m^2)
1.45	0.887×10^{-4}	0.254	0.777×10^{-5}
1.45	0.887×10^{-4}	0.508	1.554×10^{-5}
1.45	0.887×10^{-4}	1.450	4.437×10^{-5}
2.21	1.353×10^{-4}	0.254	0.777×10^{-5}
		(slit width for both nozzles: 30.6 mm)	

Results of experimental conditions	
Quantity	Range
Air/liquid mass ratio	0.3–5.0
Liquid mass flow rate	11.34–37.80 g/s
Liquid exit velocity	0.3–4.9 m/s
Air exit velocity	105–313 m/s
Exit Mach number	0.22–1.0
Underexpansion ratio[a]	1.0–1.5
Stagnation pressure	108.2–294.2 kPa

[a]Defined as the ratio of the underexpanded air density to the ambient air density.

actions without the complexity of three-dimensional configurations. The spray is nearly two-dimensional along the x-y plane. When a laser beam is aligned perpendicular to the x-y plane of the spray, laser diffraction measurements can be made with less interference by obscuration from multiple particles than in a concentric spray. Photographs of flow patterns of the two-dimensional spray are shown in Fig. 2a and b. Without air flow (Fig. 2a), the edges of the liquid film converge toward the axis due to the contractive action of surface tension [17] and the liquid film eventually transforms into a cylindrical stream. With air flow, the liquid film is rapidly broken up by the shearing action of the impinging air jets and a nearly two-dimensional expanding spray is formed as shown in Fig. 2b.

The width of the liquid and air slits of the atomizer can be varied to allow independent variation of the liquid film and air film thicknesses. The various combinations of air and liquid slit sizes are presented in Table 1, together with the range of experimental conditions. Applying isentropic flow assumptions, an analysis has been made of the flow conditions in the converging air nozzle. Specific air mass flow rate can be expressed in terms of air properties at the nozzle exit [18], i.e.,

$$\frac{\dot{m}_{\text{air}}}{A} = P_1 M_1 \sqrt{\frac{\gamma}{RT_1}} \tag{1}$$

in which A represents the nozzle exit (throat) area and the nozzle exit Mach number M_1 is given for a perfect gas by

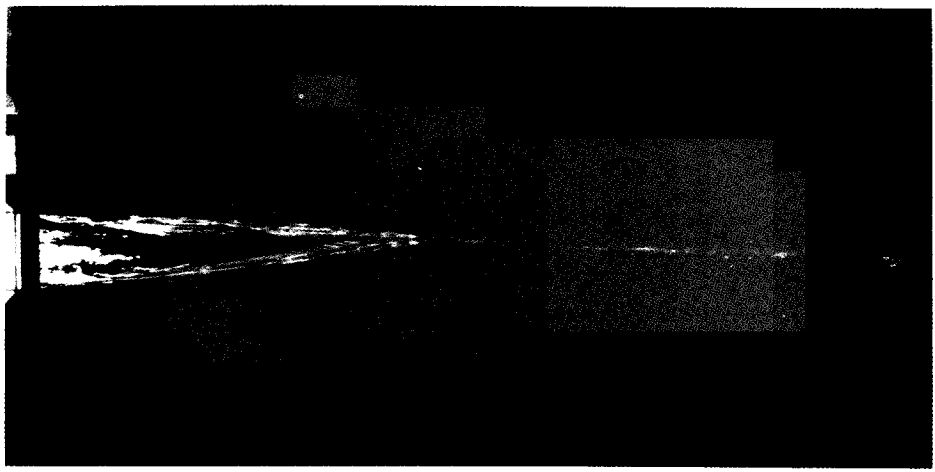

a) no air

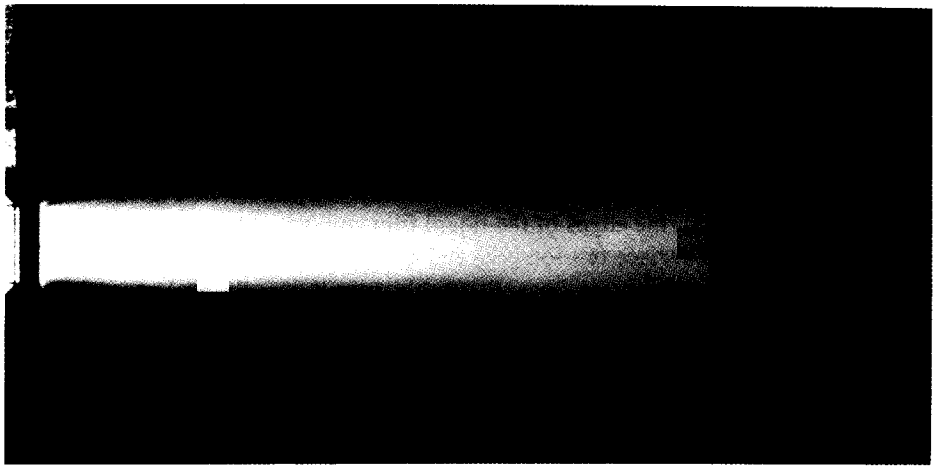

b) with air

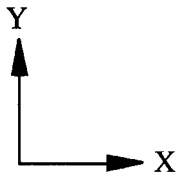

Fig. 2 Flow patterns of the two-dimensional spray: (a) without air flow and (b) with air flow.

$$M_1 = \sqrt{\left[\left(\frac{P_0}{P_1}\right)^{\gamma-1/\gamma} - 1\right]\left(\frac{2}{\gamma - 1}\right)} \tag{2}$$

where P_0 denotes stagnation pressure and the subscript 1 denotes a property at the nozzle exit. For air, the specific heat ratio $\gamma = 1.4$ and the gas constant $R = 287.07$ J/kg K.

The variations of specific air mass flux $\dot{m}_{air}/A$ and the nozzle exit Mach number M_1 are plotted as a function of stagnation pressure P_0 in Fig. 3. The stagnation pressure P_{0c}, at which flow choking is initiated, was calculated to be 191.5 kPa. When the stagnation pressure is increased, the Mach number increases until the air flow is choked ($M_1 = 1$). With further increase in stagnation pressure the exit Mach number remains unity but the air density increases progressively due to the compression, and so the air mass flux continues to increase.

Shadowgraphic Visualization Technique

The optical arrangement for the shadowgraphic technique is shown schematically in Fig. 4. An essential feature of the method is the use of a point-shaped light source created by the aperture. A metal-halide arc lamp was used as the light source. Light intensity variations in the shadowgraph are sensitive to changes in the second derivative of density or refractive index of the medium [19]. By inserting a knife edge, the shadowgraph system can be converted into a schlieren system that is sensitive to changes in the

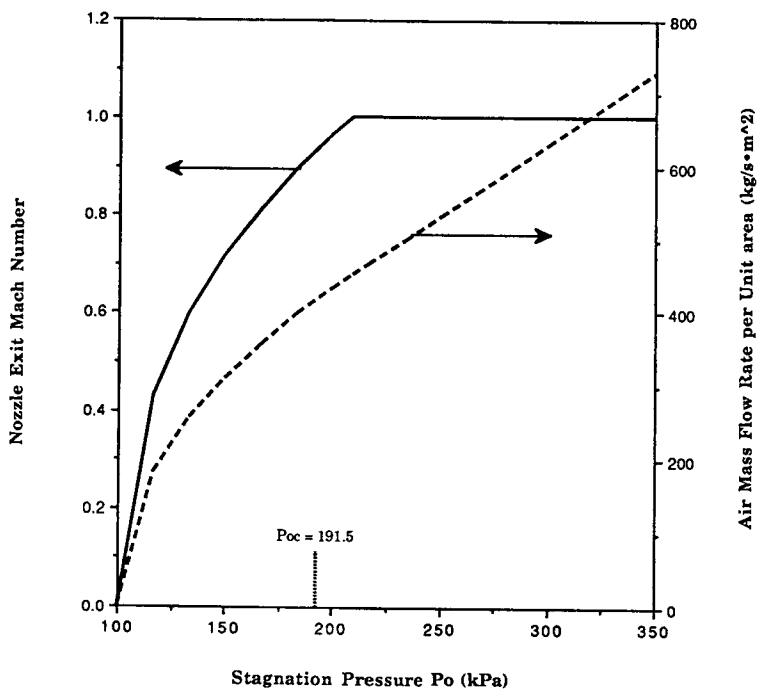

Fig. 3 Air mass flux $\dot{m}_{air}/A$ and the nozzle exit Mach number M_1 as a function of stagnation pressure P_0.

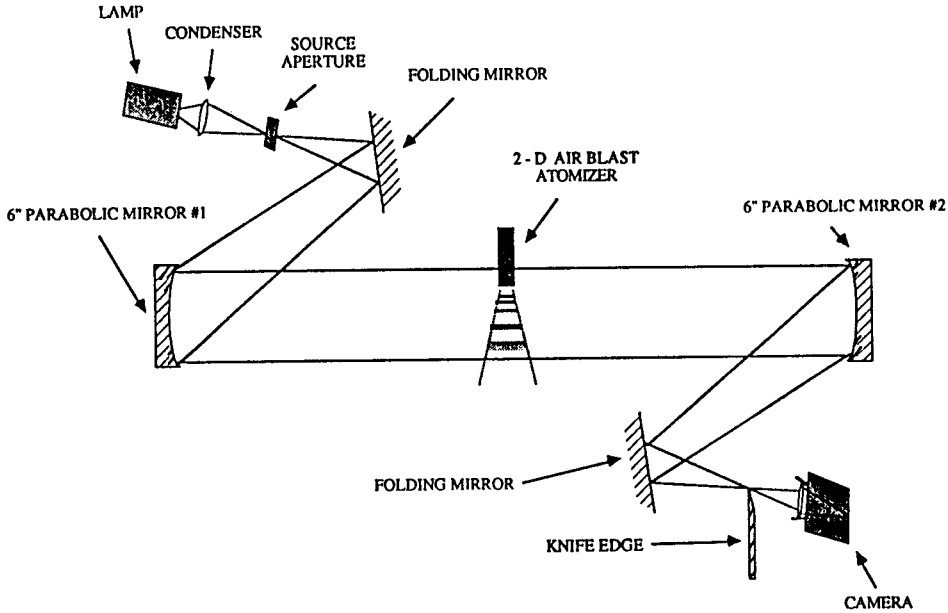

Fig. 4 Both shadowgraph and schlieren systems for flow visualization.

first derivative of the density of the medium. Although both systems have been used to visualize the shock wave patterns, only shadowgraphic visualization results are presented in this paper since they provide better-quality pictures than schlieren photographs for our application.

Drop-Sizing Technique

Figure 5 illustrates schematically the laser diffraction particle-sizing technique, which has been well established for the past decade. The basic principle of the technique is the use of Fraunhofer diffraction theory; i.e., the scattered angle of diffracted light decreases with increase in diameter of the scattering particles [20]. Distributed light energy scattered by individual particles of different diameters is detected by a series of

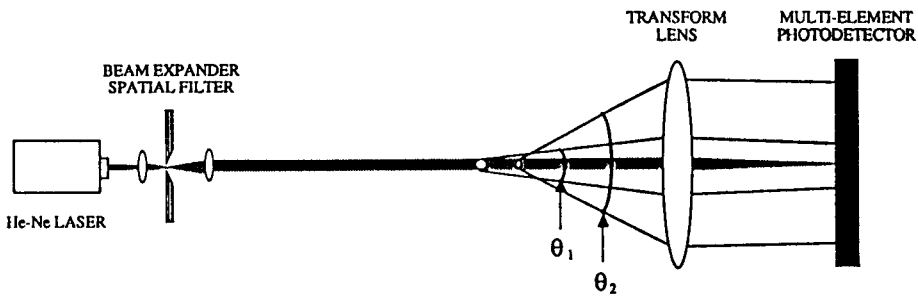

Fig. 5 Schematic illustration of the principle of the Malvern Fraunhofer diffraction particle-sizing technique.

annular ring-shaped photodiodes and is converted into a size distribution function using statistical iterations. Since the detector unit detects scattered light from all particles passing through the laser beam approximately within the focal length of the receiving lens, the method is called a line-of-sight sizing technique [21].

Measurements were made of the Sauter mean diameter (SMD) of atomized droplets, applying the Rosin-Rammler two-parameter model [22], which is defined as

$$Q = 1 - \exp - \left(\frac{D}{D_0}\right)^q \tag{3}$$

where Q is the volume fraction of particles of diameter less than D, and q and D_0 are the two parameters that are obtained from statistical iteration of the measured light energy distribution. SMD is defined as the diameter of a drop having the same volume/surface ratio as the entire spray, i.e.,

$$\text{SMD} = \frac{\Sigma_i n_i D_i^3}{\Sigma_i n_i D_i^2} \tag{4}$$

where n_i represents the number concentration of droplets of diameter D_i.

When q is larger than unity, SMD can be expressed in terms of the gamma function Γ with the two model parameters [23]:

$$\text{SMD} = D_0 \left[\Gamma\left(1 - \frac{1}{q}\right)\right]^{-1} \tag{5}$$

The ring diodes in the detector unit were carefully calibrated according to the method developed by Dodge [24]. After the calibration, the accuracy of the instrument was checked with a standard calibrating reticle (D_0 = 50 μm and q = 3.0) and the result showed an accuracy better than 5% [25]. For the case of dense sprays with high obscuration (higher than 50% in general), multiple scattering of laser light may result in measurements of mean drop size that are smaller than the true mean. The two distribution parameters of the Rosin-Rammler model were corrected to allow for multiple scattering using the correction equations suggested by Felton et al. [26]. SMD was calculated based on these corrected distribution parameters q and D_0 with Eq. (5) as long as q is larger than unity. Although Felton showed that his correction equation may be used for obscurations up to 95%, the data for obscurations only up to 90% are presented with the correction.

RESULTS AND DISCUSSION

Shock Wave Patterns

Figure 6 shows typical shadowgraphs of shock wave patterns for single (Fig. 6a) and double (Fig. 6b) air jets with an air slit size of 1.45 mm and no liquid. The air slit was oriented in parallel with the light passage so that the recorded plane was perpendicular to the y direction. For the nearly adapted single air jet (P_0 = 198 kPa), shock wave

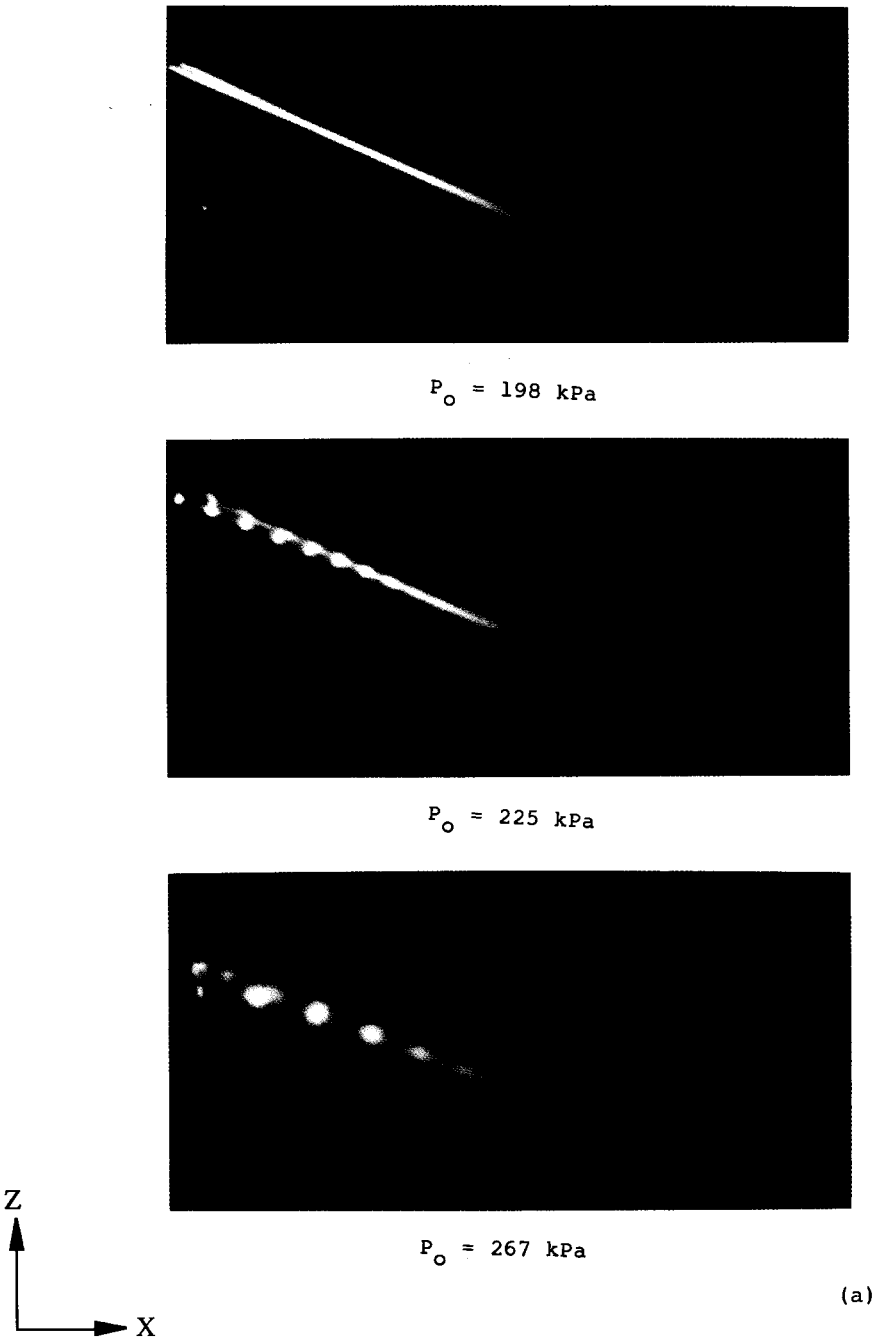

Fig. 6 Shadowgraph visualization of shock wave patterns for air jets with air slit size of 1.4 mm and no liquid: (a) single air jets, P_0 = 198, 225, and 267 kPa; (b) double air jets, P_0 = 198, 225, and 267 kPa.

P_o = 198 kPa

P_o = 225 kPa

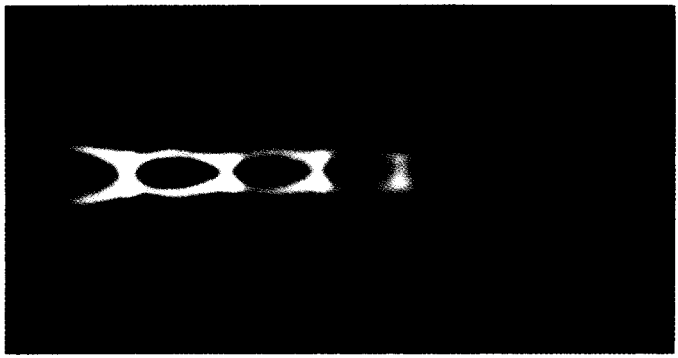

P_o = 267 kPa

(b)

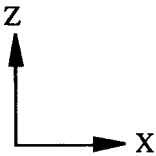

Fig. 6B Shadowgraph visualization of shock wave patterns for air jets with air slit size of 1.4 mm and no liquid: double air jets, P_0 = 198, 225, and 267 kPa.

patterns have not yet been distinctively observable, and the slightly underexpanded air flow diffuses according to viscous dissipation. As the stagnation pressure is progressively increased, diamond-shaped shock cell patterns become clearly observable and the size and strength of individual cells increase.

When air is supplied through both air orifices, the two jets impinge at the nozzle exit. The resulting shock patterns for the impinging jets are shown in Fig. 6b. Comparison with Fig. 6a shows that the shock structure of the double jets is significantly modified from that of the single jet as a result of impingement with the second air jet. Individual shock cells generated from each nozzle are stretched and bounced off each other, resulting in flow patterns symmetric about the axis. The bouncing distance and height increase with increase in the stagnation pressure. As we proceed downstream, the bouncing distance gradually decreases because of the viscous dissipation, and the shock patterns eventually diffuse away. The flow converts to a subsonic free jet with the growth of mixing layers downstream. The bouncing and diffusing of the underexpanded air jets are analogous to those of a "skipping stone" on a water surface corresponding to the symmetry plane of the air jets.

Using a simplified method of characteristics applied to Prandtl-Meyer expansion fans [18], an analysis has been made of the shock cell patterns of a single air jet from which the shock cell length and width, local Mach numbers, pressure, temperature, and density are determined as a function of the stagnation pressure. Isentropic flows have been assumed, and results of the calculations for $P_0 = 239.0$ kPa are shown with the schematic shock wave patterns in Fig. 7. The light intensity variations shown in the shadowgraphs are attributed to the spatial distribution of the ratio of local to ambient air density. The averaged length of the first three shock cells in each shadowgraph was measured for a range of stagnation pressures from 225.0 to 294.2 kPa, and data are compared with the calculated lengths presented as the solid curve in Fig. 8. The comparison shows good agreement over the wide range of stagnation pressure. The increased discrepancy at high stagnation pressure is due to the fact that the jet flow is no longer isentropic as the local Mach numbers (M_2 or M_3) are increased.

In the presence of liquid spray, the authors initially expected that a shadowgraphic technique was not applicable since the density ratios between liquid and air are so large that they overshadow the density variations within the air that are used to visualize shock waves, even if they exist. Surprisingly, the shadowgraphic attempt was successful in visualizing shock waves, although the recorded picture quality was poor because of light scattering and attenuation by water droplets. Figure 9a shows shock waves in the presence of water passed through the center slit of 0.254-mm thickness. Shock wave patterns are not well visualized at the nozzle exit since highly concentrated liquid sheet, ligaments, and droplets overshadow them. As we proceed downstream, where liquid becomes less concentrated, shock wave patterns become clearly visible. Apparently faster decay of shock cell patterns, compared with those in the absence of liquid, is due to the enhancement of both the shadowed light attenuation and the viscous dissipation of shock waves in the presence of liquid elements.

The Mach number in each air jet periodically varies along its shock cells and ranges from sonic to transonic when the jet is underexpanded (see Fig. 7). The maximum Mach number is attained in region 3, which is elongated to a bow-shaped region due to the impingement of the second jet in Fig. 9, and the sonic (minimum Mach number) condition is attained in region 1, two of which from the double air jets, meet

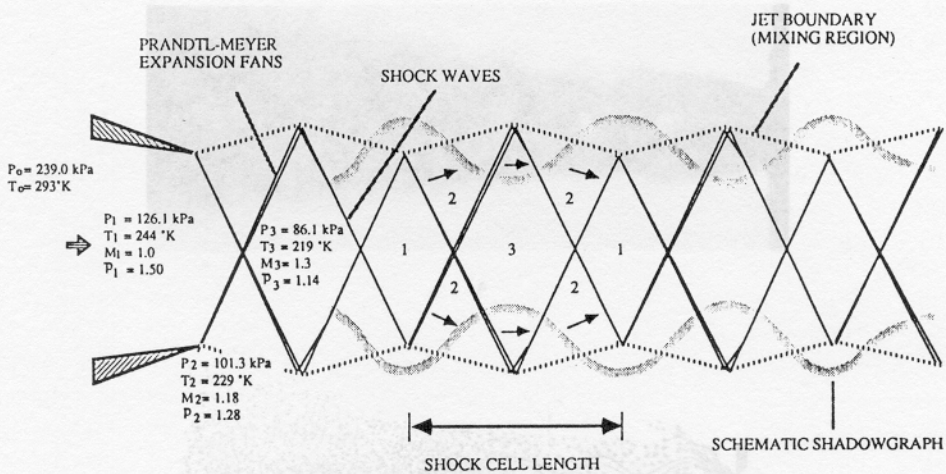

Fig. 7 Schematic illustration of underexpanded air jet at Mach number 1.3 for P_0 = 239 kPa with theoretical predictions of flow properties.

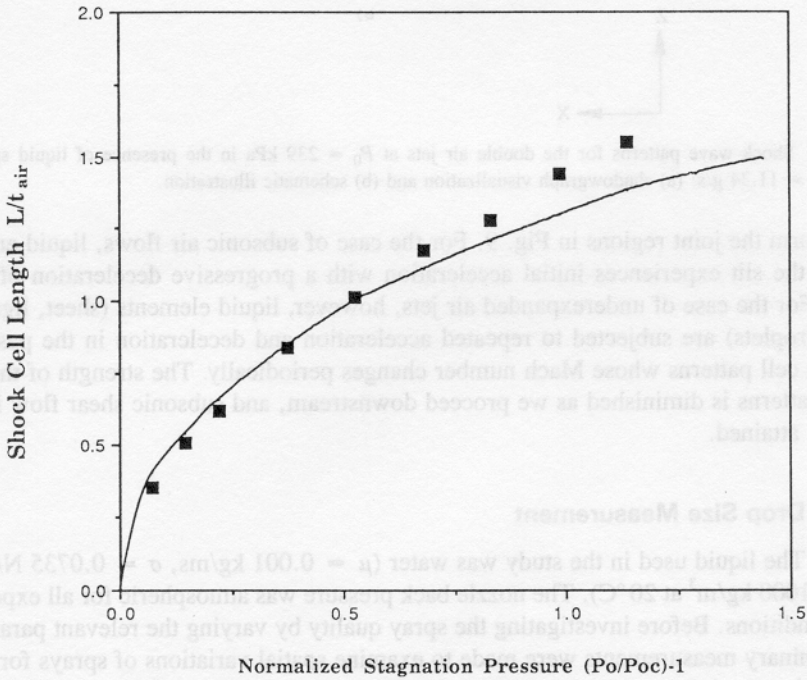

Fig. 8 Dimensionless shock cell length L/t_{air} as a function of dimensionless stagnation pressure $P_0/P_{0c} - 1$: (symbols) averaged length of the first three shock cells in shadowgraphs; (solid curve) calculated shock cell length based on the Prandtl-Meyer expansion fan theory.

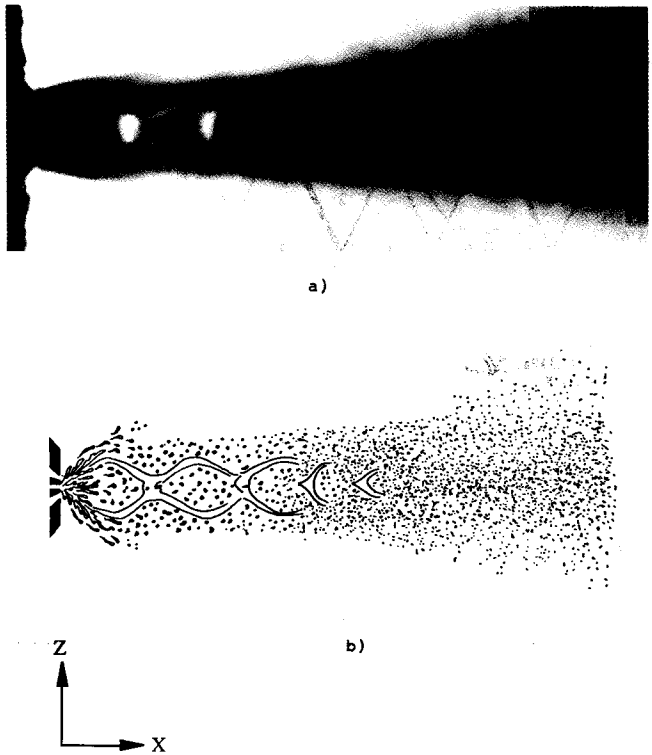

Fig. 9 Shock wave patterns for the double air jets at P_0 = 239 kPa in the presence of liquid spray with $\dot{m}_{liquid}$ = 11.34 g/s: (a) shadowgraph visualization and (b) schematic illustration.

and form the joint regions in Fig. 9. For the case of subsonic air flows, liquid emerging from the slit experiences initial acceleration with a progressive deceleration of the air jets. For the case of underexpanded air jets, however, liquid elements (sheet, ligaments, and droplets) are subjected to repeated acceleration and deceleration in the passage of shock cell patterns whose Mach number changes periodically. The strength of the shock cell patterns is diminished as we proceed downstream, and subsonic shear flow is eventually attained.

Drop Size Measurement

The liquid used in the study was water (μ = 0.001 kg/ms, σ = 0.0735 N/m, and ρ = 1000 kg/m^3 at 20 °C). The nozzle back pressure was atmospheric for all experimental conditions. Before investigating the spray quality by varying the relevant parameters, preliminary measurements were made to examine spatial variations of sprays for typical conditions and the results are presented in Figs. 10 through 12.

Figure 10 shows variations of SMD and obscuration measured at $y = z = 0$ along the spray axis (the x coordinate in Fig. 1) for air/liquid ratio = 1 with P_0 = 128.8 kPa and $\dot{m}_{liquid}$ = 22.67 g/s. The drop mean diameter decreases initially due to rapid transfer of shearing energy from the high-speed air to the liquid. As a result of this energy transfer, liquid (ligaments or drops) will be accelerated while the air is

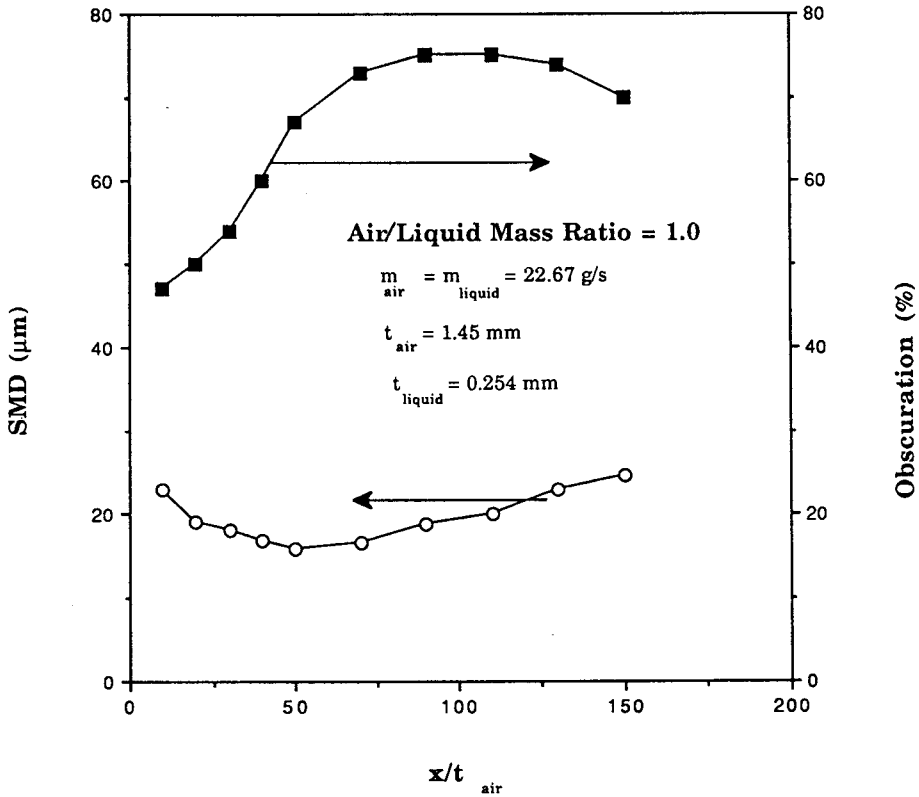

Fig. 10 Variations of Sauter mean diameter (SMD) and obscuration along the spray axis for subsonic air jets at P_0 = 128.8 kPa.

decelerated, which will increase the probability of collision and coalescence of drops. The gradual increase in SMD, after the initial decrease, is believed to be due to this increased coalescence. In addition, preferential vaporization of small droplets can contribute to increase in SMD. Obscuration is defined as

$$\text{OBS}\ (\%) = 100 \times \left(1 - \frac{\epsilon}{\epsilon_0}\right) \tag{6}$$

where ϵ and ϵ_0 denote the amount of light energy detected by the center diode in the detector unit with and without spray, respectively. One hundred percent obscuration means that the laser beam is completely scattered to all the ring diodes other than the center one. Dense sprays generally increase the obscuration. Along the length of the spray, obscuration increases as the spray diverges and becomes more dense because of the breakup of liquid elements. Farther downstream the obscuration remains nearly uniform since the spray diverges slowly, and at the same time the liquid concentration is reduced due to evaporation. A reference position of all the successive measurements was selected as x/t_{air} = 50 with t_{air} = 1.45 mm or, equivalently, x = 7.25 cm, where a minimum SMD was measured.

Measurements of SMD and obscuration along the slit axis (the y coordinate) at P_0 = 128.8 kPa were made at x = 7.25 cm and results are presented in Fig. 11. The results show nearly uniform distribution of SMD over the central 60% of the spray, where the spray may be considered two-dimensional. The significant increase in SMD near the boundaries of the spray is partially a result of the preferential evaporation of small droplets and partially a result of poor atomization due to the relatively low shear energy transfer as the boundaries are approached. As expected, the obscuration is high in the center and rapidly decreases to zero at the boundaries of the spray.

Figure 12 shows results of measurements along the z coordinate for similar conditions. The distributions of SMD and obscuration are quite symmetric about the center plane and show qualitative consistency compared to those presented in Fig. 11. The two-dimensionality of the spray is not as good in the z direction as that of the spray in the y direction, since the spray diverges more rapidly in the y-z plane than in the x-y plane. Based on the preliminary measurements, the representative SMD in the spray was measured at x = 7.25 cm, y = 0, z = 0 and the measurement plane was set perpendicular to the x-y plane; i.e., the laser beam was aligned parallel to the z axis. For fixed nozzle dimensions, the important parameters influencing SMD are air/liquid mass ratio, liquid flow rate, and relative velocity between air and liquid. By independently varying these parameters, variations of SMD were measured and results are presented in Figs. 13 and 14. All tests were conducted with an air gap of 1.45 mm and a liquid gap of 0.254 mm. In order to take into account the compressibility of underexpanded air jets, the relative

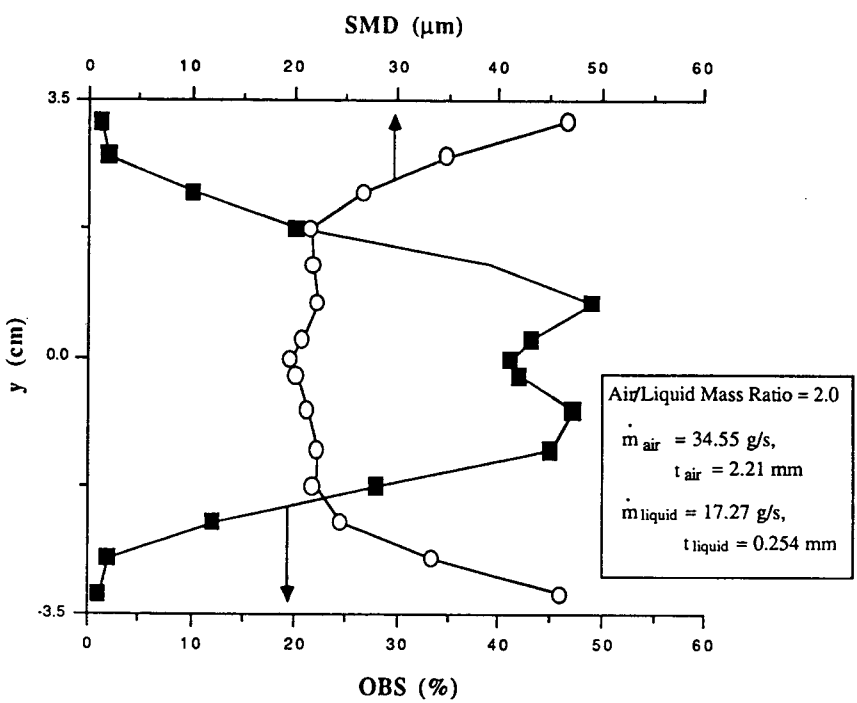

Fig. 11 Variations of SMD and obscuration along the slit axis at x = 7.25 cm for subsonic air jets at P_0 = 128.8 kPa.

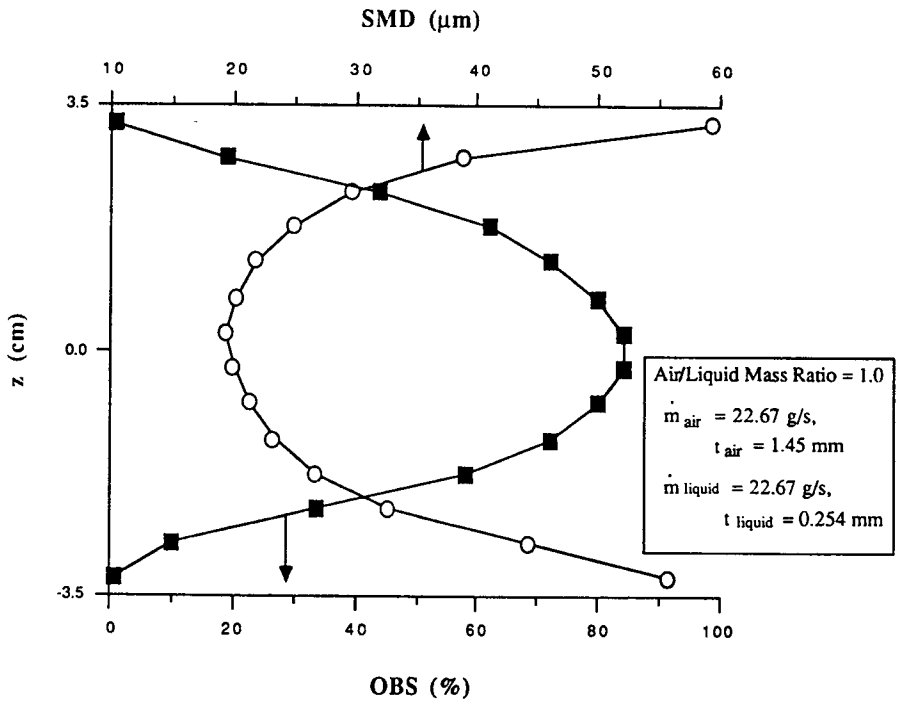

Fig. 12 Variations of SMD and obscuration along the z coordinate at x = 7.25 cm for subsonic air jets at P_0 = 128.8 kPa.

velocity is weighted by the density ratio $\bar{\rho}$, which is defined as the ratio of the air density at the nozzle exit to the ambient air density. The value of $\bar{\rho}$ is unity until the air flow is choked and is larger than unity thereafter. The open symbols represent subsonic air jets and the filled symbols represent underexpanded air jets.

Figure 13 shows results for SMD versus air/liquid mass ratio measured by increasing the air flow rate while keeping the liquid flow rate constant. For all the conditions of different liquid flow rates, the droplet SMD decreases rapidly with increases in air/liquid ratio when the air jets are subsonic. This decrease in SMD is attributed to a progressive increase of the disruptive energy of shear jets per unit liquid mass. As the sonic condition is approached, the rate of decrease in SMD slows down dramatically even if the mass or momentum flux increases in nearly a linear manner (see Fig. 3). The nearly plateaued regions for choked flows imply that a limit of atomization has been reached; i.e., the Weber number has become comparable to a critical value near the sonic condition and a further decrease in SMD becomes very difficult.

The forces determining breakup of liquid elements comprise two dimensionless groups: a Weber number We = $\rho_g U^2_{rel} D/\sigma$, which is defined as the ratio of inertial to surface tension force, and a viscosity group $N_{VI} = \mu\sqrt{\rho\sigma D}$, where ρ and ρ_g represent the density of liquid and gas, respectively; D denotes the diameter of a liquid element; U_{rel} represents the velocity of gas relative to liquid; and σ and μ are the surface tension coefficient and dynamic viscosity of the liquid, respectively. For most applications, N_{VI} is negligibly small compared to We, and the Weber number is a primary dimensionless

group for determination of liquid breakup [27]. In the present case, for example, $N_{VI} = 0.044$ with $\mu = 0.001$ kg/ms, $\rho = 1000$ kg/m^3, $\sigma = 0.0735$ N/m, and $D \approx 7 \times 10^{-6}$ m near the sonic condition, whereas We = 10 with $\rho_g = 1.1614$ kg/m^3. $U_{rel} \approx 300$ m/s, $D = 7 \times 10^{-6}$ m, and $\sigma = 0.0735$ N/m. A critical Weber number We_{crit} is a criterion below which the breakup action of the inertial force of the gas cannot overcome the holding action of surface tension of the liquid and, therefore, the liquid does not break up further. Merrington and Richardson [28] estimated We_{crit} empirically as in the range of 5 to 25. For breakup of a drop in a convective airstream after the passage of a normal shock wave, which is closely relevant to the present case, Hinze [29] has found $We_{crit} = 13$ for $N_{VI} \approx 0$. Hanson et al. [2] obtained semiempirically that $We_{crit} = 6$ for "small" viscosity and 10 for "large" viscosity with $N_{VI} = 1$ as the criterion between "small" and "large" viscosities. Therefore, near the sonic condition of the present case, the critical Weber number is reached, and a further reduction in SMD becomes very difficult even if ρ_g increases linearly due to the underexpansion.

Adelberg [30] estimated the maximum stable mass median diameter (MMD or D_{30}) of droplets generated by a liquid jet penetrating a high-speed gas stream. For the sonic condition, calculation of MMD with the Adelberg equation gives values in the range of 11.7 to 12.3 μm. Although SMD (D_{32}) has a slightly smaller value than MMD (D_{30}) for the same distribution of droplet diameters, the estimated value of the maximum stable SMD for the present case will be about 5 to 10 μm. As can be seen in Fig. 13 and others, SMD at the sonic condition is the same order of magnitude as the estimated value. This

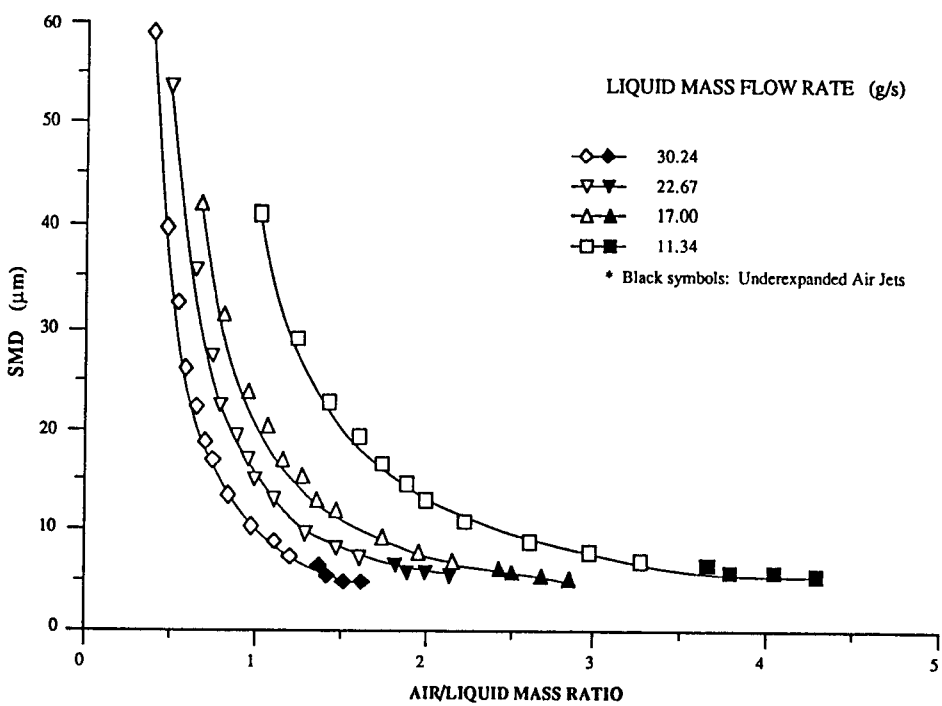

Fig. 13 SMD variations versus air/liquid mass ratio for different liquid mass flow rates for both subsonic and supersonic air flows.

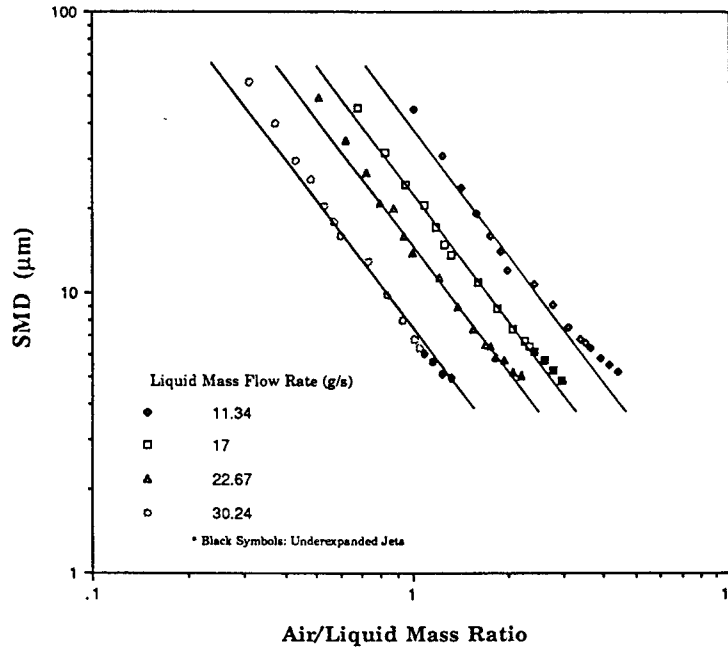

Fig. 14 Replot of the data presented in Fig. 13 on a log-log scale.

can be another indication that a critical breakup condition is nearly attained at around the sonic condition of the present configuration of the airblast atomizer.

Another important aspect to note is that for the same value of air/liquid mass ratio, SMD decreases with increases in liquid mass flow rate. As the liquid flow rate is increased while air/liquid mass ratio is kept constant, the air velocity is increased to a much greater degree than the liquid velocity because of the large density difference between air and liquid. This results in increased momentum transfer per unit liquid mass and leads to a reduced SMD as the liquid mass flow rate is increased. The relative velocity between air and liquid plays a dominant role in determining SMD for a fixed nozzle geometry.

In order to explore the correlation of SMD with air/liquid mass ratio, the data presented in Fig. 13 are replotted on a log-log scale in Fig. 14. The straight lines were drawn based on linear interpolatons of the subsonic data. The SMD values represented by filled symbols beyond the choking indicate slight deviations from the correlation lines with slower decrease of SMD with increase in air/liquid ratio. Although values of SMD appear to decrease nearly linearly even after choked flow, it should be noted that the amount of successive decrease of SMD is on the order of 1/10 μm. The correlation for SMD versus air/liquid mass ratio, $\dot{m}_{air}/\dot{m}_{liquid}$, is obtained from the interpolation as

$$\mathrm{SMD} = \left(\frac{\dot{m}_{air}}{\dot{m}_{liquid}}\right)^{-1.515} \quad (\mu\mathrm{m}) \tag{7}$$

which shows that SMD is inversely proportional to air/liquid mass ratio raised to the power of 1.515.

Results presented in Fig. 15 show the influence of relative velocity on SMD more extensively. Measurements were made varying relative velocities while keeping the air/liquid mass ratio constant. The increase of air/liquid mass ratio, for a fixed value of relative velocity, reduces SMD for lower values of relative velocities. The reduction in SMD diminishes as the air flow is choked and the shock waves appear. For the three conditions of air/liquid mass ratio, SMD shows a rapid decrease with increase in relative velocity until the air jets are choked. Further increase in relative velocity hardly changes the droplet SMD, since the critical breakup condition, i.e., the critical Weber number, is already reached.

The data from Fig. 15 are presented on a log-log scale in Fig. 16. Although deviations of the sonic data (filled symbols) are observed, most subsonic data are fairly well (with some scattering) fitted with the linear interpolation. Sauter mean diameter is inversely proportional to weighted relative air velocity to the power of 1.358, as expressed by an equation of interpolation

$$\mathrm{SMD} = 20{,}800\,(\bar{\rho}V_{\mathrm{rel}})^{-1.358} \quad (\mu\mathrm{m}) \tag{8}$$

in which V_{rel} is expressed in m/s.

The effect of variation in liquid slit width on SMD is presented as a function of weighted velocity $\bar{\rho}V_{\mathrm{rel}}$ in Fig. 17. For the three different liquid slit widths, the air slit

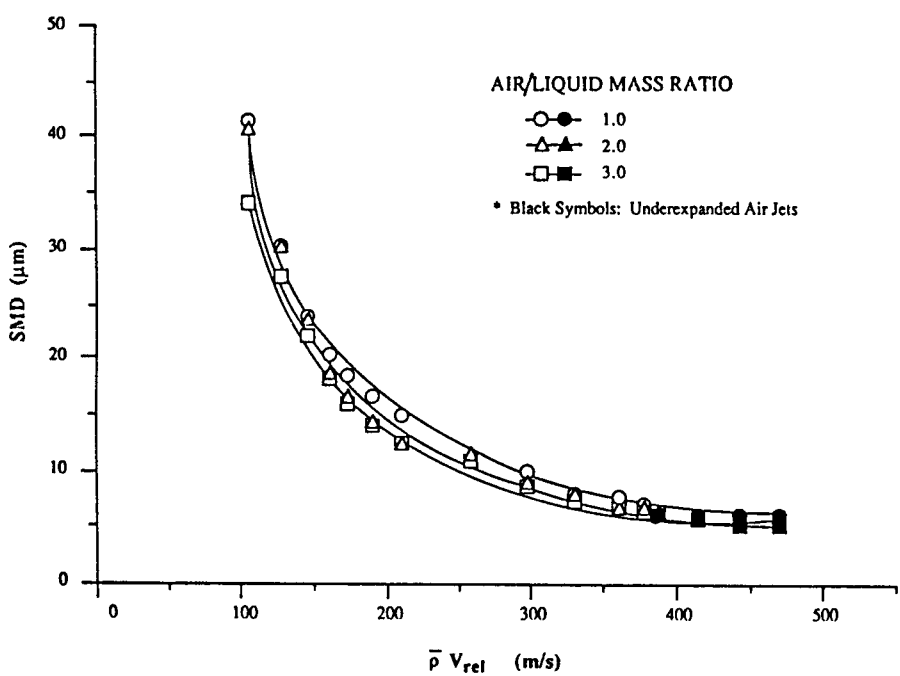

Fig. 15 SMD versus weighted relative velocity $\bar{\rho}V_{\mathrm{rel}}$ for different air/liquid mass ratios for both subsonic and supersonic air flows.

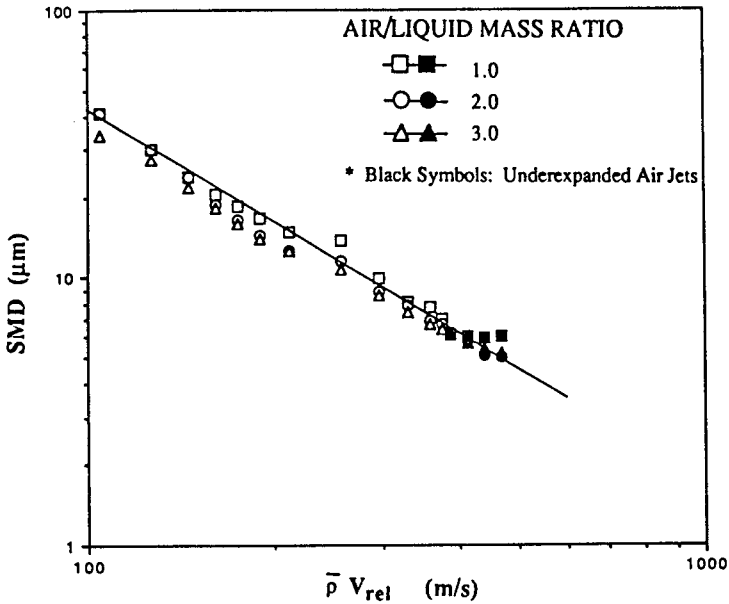

Fig. 16 Replot of the data presented in Fig. 15 on a log-log scale.

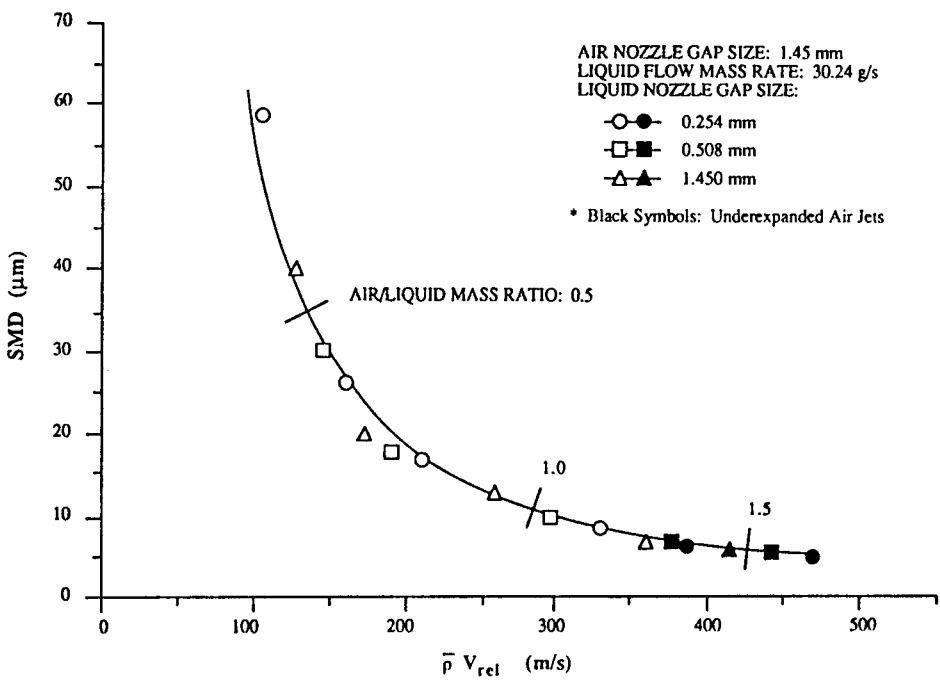

Fig. 17 SMD is independent of liquid slit size for t_{air} = 1.45 mm for both subsonic and supersonic air flows.

width was maintained fixed at 1.45 mm. All the data points of measured SMD fall on a single curve regardless of liquid slit width, showing that there is no influence of liquid gap width on atomization quality for this type of airblast atomizer. Lorenzeto and Lefebvre [9] also showed for subsonic air flows that the dependence of the slit width on SMD is not noticeable unless a liquid of extremely high viscosity is employed.

The dependence of SMD on air slit width is illustrated in Fig. 18. Two different air slit widths of 1.45 mm and 2.21 mm were studied while the liquid gap width of 0.254 mm remained constant. Again, the variation of mean drop size is not influenced within the examined range of air slit width. It is obvious from inspection of Figs. 13 through 18 that (weighted) relative air velocity to liquid velocity is the most important of the parameters influencing SMD in airblast atomizers.

SUMMARY AND CONCLUSIONS

Effects of both adapted and underexpanded air jets on airblast atomization have been investigated with a two-dimensional airblast atomizer. For subsonic (adapted) air flows, the representative SMD shows a rapid decrease with increase in the air supply pressure. The relative velocity of air to liquid is the most decisive parameter in determination of the mean drop size for air flows up to the sonic condition. Once the air flow is choked and the shock cell patterns are established, the rate of decrease in SMD slows down dramatically. Detailed examination of the force balance and the maximum stable drop size reveals that both the critical Weber number and the critical diameter of droplets have been nearly attained at the sonic condition for the atomizer employed, and a further

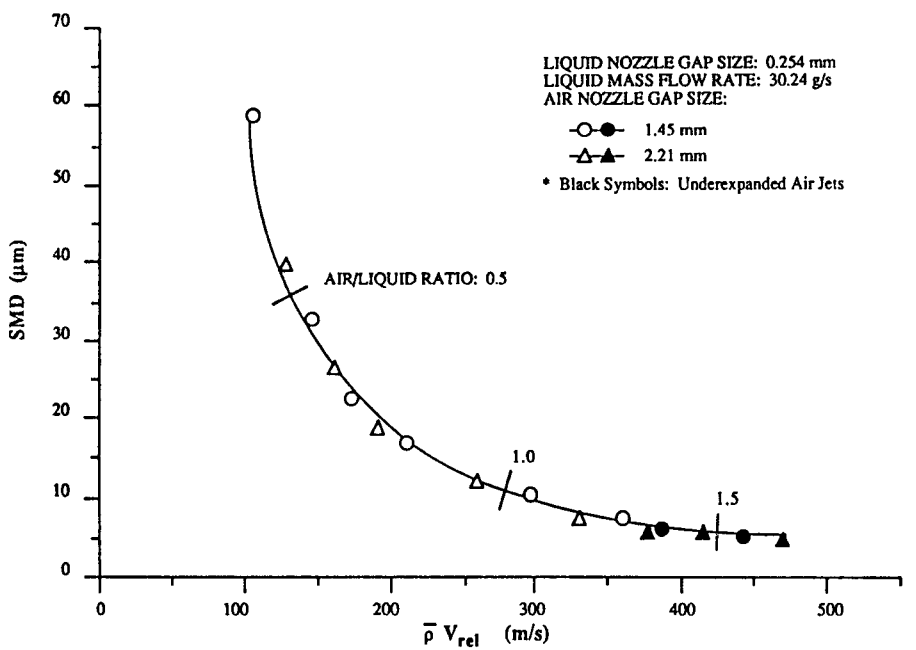

Fig. 18 SMD is independent of air slit size for t_{liquid} = 0.254 mm for both subsonic and supersonic air flows.

reduction in SMD becomes very difficult to achieve unless the air inertia is high enough to overcome the surface tension and raise the Weber number above the critical value. The evidence in this study shows that there is no special reason to create shock waves or shock cell patterns with the specific aim of efficient improvement of atomization. Based on the present investigation, it is postulated that the noncontinuous shear action of repeated acceleration and deceleration in the established shock cell patterns may reduce, or at least does not enhance, the atomization efficiencies, which can be defined as the ratio of the inverse mean diameter of atomized aerosols to the power needed to operate the atomizer compressor. In order to investigate the postulate together with a comprehensive study of the critical Weber number, it would be necessary to employ a supersonic (up to a Mach number of 3 or 4) airblast atomization configuration.

REFERENCES

1. A. W. Lefebvre, *Gas Turbine Combustion,* chap. 10, McGraw-Hill, New York, 1983.
2. A. R. Hanson, E. G. Domich, and H. S. Adams, Shock Tube Investigation of the Breakup of Drops by Air Blasts, *Phys. Fluids,* vol. 6, no. 8, pp. 1070–1080, 1963.
3. A. A. Ranger and J. A. Nicholls, Aerodynamic Shattering of Liquid Drops, *AIAA J.,* vol. 17, no. 2, pp. 285–290, 1969.
4. A. A. Ranger and J. A. Nicholls, Atomization of Liquid Droplets in a Convective Gas Stream, *Int. J. Heat/Mass Transfer,* vol. 15, pp. 1203–1211, 1972.
5. T. Yoshida, A. Wierzba, and K. Takayama, Breakup and Interaction of Two Droplet Columns in a Shock Wave Induced High-Speed Air Flow, *ICLASS,* pp. 101–108, Sendai, Japan, 1988.
6. K. Y. Kim and W. R. Marshall, Drop-Size Distributions from Pneumatic Atomizers, *AIChE J.,* vol. 17, no. 3, pp. 575–584, 1971.
7. A. A. Rizkalla and A. H. Lefebvre, Influence of Liquid Properties on Airblast Atomizer Spray Characteristics, *J. Eng. Power,* pp. 173–179, 1975a.
8. A. A. Rizkalla and A. H. Lafebvre, Influence of Liquid Properties on Airblast Atomizer Spray Characteristics, *J. Fluids Eng.,* vol. 97, no. 3, pp. 316–320, 1975b.
9. G. E. Lorenzetto and A. H. Lefebvre, Measurements of Drop Size on a Plain-Jet Airblast Atomizer, *AIAA J.,* vol. 15, no. 7, pp. 1006–1010, 1977.
10. A. C. Styles and N. A. Chigier, Combustion of Air Blast Atomized Spray Flames, 16th Symposium on Combustion, pp. 619–630, The Combustion Institute, Pittsburgh, 1977.
11. N. K. Rizk and A. H. Lefebvre, The Influence of Liquid Film Thickness on Airblast Atomization, *J. Eng. Power,* vol. 102, pp. 706–710, 1980.
12. A. H. Shapiro, *The Dynamics and Thermodynamics of Compressible Fluid Flow,* vols. 1 and 2, pp. 81–94, 449–456, Ronald Press, 1954.
13. M. Van Dyke, *An Album of Fluid Motion,* p. 98, Parabolic Press, 1982.
14. H. C. Simmons, The Prediction of Sauter Mean Diameter for Gas Turbine Fuel Nozzles of Different Types, ASME Paper 79-WA/GT-5, 1979.
15. N. A. Chigier, *Energy, Combustion, and Environment,* chap. 7, McGraw-Hill, New York, 1981.
16. H. G. Barth, *Modern Methods of Particle Size Analysis,* chap. 5, Wiley, New York, 1984.
17. H. N. V. Temperly and D. H. Trevena, *Liquids and Their Properties,* pp. 163–190, Wiley, New York, 1978.
18. J. E. A. John, *Gas Dynamics,* pp. 35–54, 123–129, and 307–309, Allyn and Bacon, 1969.
19. W. Merzkirch, *Flow Visualization,* pp. 115–149, Academic Press, Orlando, Fla., 1987.
20. E. Hecht, *Optics,* chap. 10, Addison-Wesley, Reading, Mass., 1974.
21. E. D. Hirleman, V. Oechsle, and N. A. Chigier, Response Characteristics of Laser Diffrac-

tion Particle Size Analyzers: Optical Sample Volume Extent and Lens Effects, *Opt. Eng.*, vol. 23, no. 5, pp. 610–619, 1984.

22. P. Rosin and E. Rammler, *The Laws Governing the Fineness of Powdered Coal*, pp. 29–36, Institute of Fuel, 1933.
23. R. A. Mugele and H. D. Evans, Droplet Size Distribution in Sprays, *Ind. Eng. Chem.*, vol. 43, no. 6, pp. 1317–1324, 1951.
24. L. G. Dodge, Calibration of the Malvern Particle Sizer, *Appl. Opt.*, vol. 23, no. 14, pp. 2415–2419, 1984.
25. E. D. Hirleman and L. G. Dodge, Performance Comparison of Malvern Instruments Laser Diffraction Drop Size Analyzers, *ICLASS 85*, extended abstract, 1985.
26. P. G. Felton, A. A. Hamidi, and A. K. Aigal, Measurements of Drop Size Distribution in Dense Sprays by Laser Diffraction, *ICLASS*, vol. 2, 1985.
27. J. O. Hinze, Fundamentals of the Hydrodynamic Mechanism of Splitting in Dispersion Processes, *AIChE J.*, vol. 1, no. 3, pp. 289–295, 1955.
28. A. C. Merrington and E. G. Richardson, The Breakup of Liquid Jets, *Proc. Phys. Soc. London*, vol. 59, no. 1, 1947.
29. J. O. Hinze, Critical Speeds and Sizes of Liquid Globules, *Appl. Sci. Res.*, vol. A1, pp. 273–288, 1948.
30. M. Adelberg, Mean Drop Size Resulting from the Injection of a Liquid Jet into a High-Speed Gas Stream, *AIAA J.*, pp. 1143–1147, 1968.
31. S. Nukiyama and Y. Tanasawa, Experiments on the Atomization of Liquids in an Airstream, *Trans. Soc. Mech. Eng. Jpn.*, vol. 5, pp. 68–75, 1939.